Table II. Complications after pancreaticoduodenectomy

Parameter	*Nonwrapping group* (n = *1,679*)	*Wrapping group* (n = *918*)*	P *value*
Pancreatic fistula			
All grades	627 (37.3)	393 (42.8)	.006
Grade B + C	281 (16.7)	198 (21.6)	.002
Delayed gastric empting	182 (10.8)	117 (12.7)	.146
Bile leakage	52 (3.1)	29 (3.2)	.931
Intra-abdominal abscess	179 (10.7)	111 (12.1)	.269
Intra-abdominal hemorrhage†			
Early	32 (1.9)	14 (1.5)	.482
Late	22 (1.3)	18 (2.0)	.198
Wound infection	151 (9.0)	115 (12.5)	.005
Other organ complications			
Respiratory	76 (4.6)	43 (4.7)	.859
Cardiac	25 (1.5)	28 (3.1)	.007
Vascular	24 (1.4)	20 (2.2)	.157
Renal	17 (1.0)	4 (0.4)	.117
Mortality	22 (1.3)	9 (1.0)	.459
Postoperative hospital stay, days (mean ± SD)	38.0 ± 37.9	41.3 ± 30.1	.014

*Wrapping of pancreatic anastomosis or vessels, including hepatic artery, using omentum or falciform ligament.
†Early intra-abdominal hemorrhage indicates incomplete hemostasis and a failure of carrying out sufficient intraoperative management. It was defined as occurring within 3 days after pancreaticoduodenectomy, and it was not associated with any other postoperative complications. Late intra-abdominal hemorrhage is associated with other postoperative complications, including pancreatic fistula and intra-abdominal abscess.

Table III. Postoperative drainage after pancreaticoduodenectomy

		*Wrapping group**	
Parameter	*Nonwrapping group* (n = *1,679*)	*Falciform ligament* (n = *219*)	*Omentum* (n = *699*)
Amylase level of postoperative drainage fluid (IU/l)			
POD1	4,405 ± 14,129	4,802 ± 17,644	4,950 ± 13,324
POD3	2,924 ± 2,963	2,077 ± 10,947	1,317 ± 2,963†
POD4	1,384 ± 6,876	327 ± 639	1,395 ± 8,227

*Wrapping of pancreatic anastomosis or vessels, including hepatic artery, using omentum or falciform ligament.
†$P = .027$ (nonwrapping versus omentum).
POD, Postoperative day.

DISCUSSION

This study was a report with a large number of patients on the effect of omentum wrapping or falciform ligament after a PD by a retrospective analysis after the report of ISGPF definition.[16] Each institution had their own criteria for pancreatic fistula before the publication of the definition of pancreatic fistula by an ISGPF. Therefore, it was difficult to compare the incidence of pancreatic fistula. The members of the JSPS now share the same definition of pancreatic fistula, and we can accumulate clinical data to compare the incidence of pancreatic fistula by using this common definition. These data were collected between January 2006 and June 2008. However, only 65% of the institutions could respond to the survey, because 35% of the institutions do not have database systems that can evaluate the incidence of pancreatic fistula according to the ISGPF criteria. Seven independent risk factors were identified for grade B + C pancreatic fistula, 4 factors for early intra-abdominal hemorrhage, and 2 factors for late intra-abdominal hemorrhage. Although the evaluation of delayed gastric emptying and intra-abdominal hemorrhage should be based on grading of ISGPS,[21,22] this study was conducted as a retrospective study, and it was difficult to accumulate sufficient data based on the ISGPS criteria that were reported in 2007.

The incidence of pancreatic fistula was significantly higher in the wrapping group in comparison to the nonwrapping group; moreover, the incidence of grade B + C pancreatic fistula was also higher in the wrapping group. However, the amylase level of the drainage fluid was lower in

Table IV. Complications according to the material used by wrapping

Parameter	*Nonwrapping group* (n = *1,679*)	*Wrapping group**			
		Falciform ligament, (%) (n = *219*)	P *value*†	*Omentum, (%)* (n = *699*)	P *value*†
Pancreatic fistula					
All grades	627 (37.3)	72 (32.8)	.197	321 (45.9)	<.001
Grade B + C	281 (16.7)	31 (14.2)	.332	167 (23.9)	<.001
Delayed gastric empting	182 (10.8)	25 (11.4)	.797	92 (13.2)	.106
Bile leakage	52 (3.1)	6 (2.7)	.773	23 (3.3)	.806
Intra-abdominal abscess	179 (10.7)	33 (15.1)	.051	78 (11.2)	.722
Intra-abdominal hemorrhage					
Early	32 (1.9)	3 (1.4)	.791	11 (1.6)	.580
Late	22 (1.3)	4 (0.5)	.532	14 (2.0)	.208
Wound infection	151 (9.0)	26 (11.8)	.168	89 (12.7)	.006
Other organ complications					
Respiratory	76 (4.6)	8 (3.7)	.554	35 (5.0)	.613
Cardiac	25 (1.5)	5 (2.3)	.382	23 (3.3)	.004
Vascular	24 (1.4)	8 (3.7)	.025	12 (1.7)	.601
Renal	17 (1.0)	1 (0.5)	.712	3 (0.4)	.156
Mortality	22 (1.3)	2 (0.9)	>.999	7 (1.0)	.532

*Wrapping of pancreatic anastomosis or vessels, including hepatic artery, using omentum or falciform ligament.
†Versus nonwrapping group.

Table V. Complications according to the location of wrapping

Parameter	*Nonwrapping group, (%)* (n = *1,679*)	*Wrapping group**			
		Vessels, (%) (n = *552*)	P *value*†	*Anastomosis,‡ (%)* (n = *366*)	P *value*†
Pancreatic fistula					
All grades	627 (37.3)	223 (40.4)	.200	170 (46.4)	.001
Grade B + C	281 (16.7)	110 (19.9)	.087	88 (24.0)	.001
Delayed gastric empting	182 (10.8)	52 (11.2)	.798	55 (15.1)	.023
Bile leakage	52 (3.1)	18 (3.3)	.848	11 (3.0)	.927
Intra-abdominal abscess	179 (10.7)	55 (9.9)	.643	56 (15.3)	.012
Intra-abdominal hemorrhage					
Early	32 (1.9)	4 (0.7)	.056	10 (2.7)	.313
Late	22 (1.3)	8 (1.4)	.806	10 (2.7)	.047
Wound infection	151 (9.0)	61 (11.1)	.153	54 (14.8)	.001
Other organ complications					
Respiratory	76 (4.6)	22 (4.0)	.591	21 (5.7)	.323
Cardiac	25 (1.5)	12 (2.2)	.274	16 (4.4)	<.001
Vascular	24 (1.4)	10 (1.8)	.525	10 (2.7)	.077
Renal	17 (1.0)	1 (0.2)	.059	3 (0.3)	.734
Mortality	22 (1.3)	6 (1.1)	.683	3 (0.8)	.602

*Wrapping of vessels, including hepatic artery, using omentum or falciform ligament.
†Versus nonwrapping group.
‡Pancreaticojejunostomy or pancreaticogastrostomy using either the omentum or falciform ligament.

patients with omental wrapping than that with other procedures. It might be suggested that the omental wrapping would disturb the drainage of oozing pancreatic juice, and that this may cause damage of the omentum. Indeed, omental wrapping is associated with complications, such as intestinal obstruction, necrosis of the omentum, and infection.[20]

A soft pancreas is susceptible to postoperative intra-abdominal hemorrhage, and a late intra-abdominal hemorrhage is a lethal complication. Omentum wrapping influenced the occurrence of intra-abdominal hemorrhage, which might be related to omentum wrapping, which is performed to protect skeletonized vessels when the surgeon considers the vessels to be fragile during an operation.

Table VI. Univariable analysis for pancreatic fistula

Parameter	*Pancreatic fistula**		P *value*
	With (n = *479*)	*Without* (n = *2,118*)	
Age, y (≥70/<70)	221/258	862/1,256	.029
Gender (male/female)	321/158	1,238/880	.010
Albumin, g/dL (≥3.5/<3.5)	354/108	1,674/383	.020
AST, IU/L (>40/<40)	211/257	807/1,261	.016
ALT, IU/L (>40/<40)	253/215	987/1,083	.013
Amylase, IU/L (>180/<180)	52/406	307/1,709	.034
Preoperative biliary drainage (yes/no)	248/231	973/1,145	.021
Pylorus preservation (yes/no)	282/197	1,118/1,000	.018
Extended resection (yes/no)	384/86	1,788/287	.013
Operation time, min (>600/<600)	116/354	378/1,693	.001
Blood loss, mL (>1,500/<1,500)	119/359	470/1,632	.233
Pancreatic texture (hard/soft)	389/90	1,070/1,048	<.001
Anastomosis (P-J/P-G)	439/40	1,876/242	.051
Duct-to-mucosal anastomosis (yes/no)	372/107	1,675/443	.491
Pancreatic stent (yes/no)	402/77	1,639/479	.002
Wrapping			<.001
Falciform ligament at pancreaticoenterostomy	5	3	
Falciform ligament at vessels	67	144	
Omentum at pancreaticoenterostomy	165	193	
Omentum at vessels	156	185	
No	627	1,052	

*Grade B + C pancreatic fistula according to the International Study Group of Pancreatic Fistula.
ALT, Alanine aminotransferase; *AST*, aspartate aminotransferase; *P-G*, pancreaticogastrostomy; *P-J*, pancreaticojejunostomy.

Table VII. Univariable analysis for intra-abdominal hemorrhage

Parameter	*Early intra-abdominal hemorrhage*			*Late intra-abdominal hemorrhage*		
	With (n = *46*)	*Without* (n = *2,551*)	P *value*	*With* (n = *40*)	*Without* (n = *2,557*)	P *value*
Age, y (≥70/<70)	25/21	1,058/1,493	.079	16/24	1,067/1,490	.826
Gender (male/female)	35/11	1,534/1,027	.025	32/8	1,527/1,030	.009
Albumin, g/dL (≥3.5/<3.5)	35/10	1,993/481	.641	29/11	1,999/480	.197
AST, IU/L (>40/<40)	20/26	998/1,492	.641	13/26	1,005/1,492	.382
ALT, IU/L (>40/<40)	25/21	1,215/1,277	.452	17/22	1,223/1,276	.507
Extended resection (yes/no)	35/10	2,137/363	.148	34/5	2,138/368	.744
Operation time, min (>600/<600)	18/30	478/2,017	.008	13/27	481/2,020	.035
Blood loss, mL (>1,500/<1,500)	15/31	574/1,960	.111	13/27	576/1,964	.142
Blood transfusion (yes/no)	27/18	776/1,642	<.001	9/27	794/1,633	.327
Pancreatic texture (hard/soft)	38/8	1,421/1,130	<.001	34/6	1,425/1,132	<.001
Anastomosis (P-J/P-G)	40/6	2,275/276	.630	35/5	2,280/277	.616
Duct-to-mucosal anastomosis (yes/no)	34/12	2,013/538	.411	31/9	2,016/541	.837
Pancreatic stent (yes/no)	38/8	2,003/548	.503	38/2	2,003/554	.011
Wrapping (yes/no)	14/32	904/1,647	<.001	22/18	1,657/900	.198
Omentum	11	688	.901	14	685	.562
At panceaticoenteric anastomosis	10	356	.109	10	356	.209

ALT, Alanine aminotransferase; *AST*, aspartate aminotransferase; *P-G*, pancreaticogastrostomy; *P-J*, pancreaticojejunostomy.

Surgeons might therefore have chosen to use wrapping for inappropriate cases or when they suspected an increased likelihood of leakage. If surgeons choose to use wrapping in worst cases, a high incidence of pancreatic fistula should be indicated in both omental wrapping and falciform ligament groups.

This study has revealed that wrapping using the omentum did not decrease the incidence of pancreatic fistula. However, this study has several

Table VIII. Risk factors for postoperative pancreatic fistula after pancreaticoduodenectomy according to a multivariable analysis

Predictor	P *value*	*Odds ratio (95% CI)*
Gender (male)	<.001	1.508 (1.200–1.896)
Albumin (<3.5 g/dL)	.035	1.332 (1.021–1.738)
Pancreas texture (soft)	<.001	4.129 (3.139–5.339)
Operation time (≥600 minutes)	.031	1.345 (1.027–1.761)
Extended resection	.013	1.461 (1.084–1.969)
Pylorus preservation	.032	1.276 (1.021–1.595)
Wrapping		
Omentum at pancreaticoenterostomy	.040	1.378 (1.104–1.871)
Omentum at vessels	.005	1.555 (1.141–2.120)

CI, Confidence interval.

limitations because it was a multicenter study using retrospective data collection, which makes it a potential source for significant bias. This study indicated that the usage of an omental flap does not reduce the occurrence of complications after PD, including the incidence of pancreatic fistula. A further validation study is therefore necessary to evaluate the efficacy of wrapping for PD.

The authors are especially grateful to the 91 leading Japanese institutions that kindly took part in the survey. These institutions are listed here:

Aichi Medical University, Department of Surgery; Division of Gastroenterological Surgery
Akita City Hospital, Department of Surgery
Asahikawa Medical College, Department of Gastroenterological Surgery
Chiba Cancer Center, Department of Gastroenterological Surgery
Chiba Rosai Hospital, Department of Surgery
Dokkyo Medical University, Department of Surgery II
Fujita Health University School of Medicine, Department of Biliary Pancreatic Surgery
Fukuoka University Faculty of Medicine, Department of Surgery
Fukui Red Cross Hospital, Department of Surgery
Fukui Saiseikai Hospital, Department of Surgery
Hachioji-Shokaki Hospital, Department of Surgery
Hamamatsu University School of Medicine, Department of Surgery II
Hino Municipal Hospital, Department of Surgery
Hirosaki University School of Medicine, Department of Surgery II
Hiroshima City Hospital, Department of Surgery
Hiroshima University Graduate School of Biomedical Sciences, Department of Surgery, Division of Clinical Medical Science
Hiroshima University Graduate School of Biomedical Sciences, Department of Surgery, Division of Frontier Medical Science
Hokkaido University Graduate School of Medicine, Department of General Surgery
Hyogo College of Medicine, Department of Surgery 1
Ise Municipal General Hospital, Department of Surgery
Itabashi Chuo Medical Center, Department of Surgery
Iwate Medical University School of Medicine, Department of Surgery
Jichi Medical University, Department of Surgery
Jikei University School of Medicine, Department of Surgery
Jikei University School of Medicine, Aoto Hospital, Department of Surgery
Jikei University, Daisan Hospital, Department of Surgery
Jikei University, Kashiwa Hospital, Department of Surgery
Kagawa University, Faculty of Medicine, Department of Gastroenterological Surgery
Kagoshima Medical Association Hospital, Department of Surgery
Kagoshima University, Department of Surgical Oncology
Kanazawa Medical University Hospital, Department of surgical Oncology
Kanazawa University Graduate School of Medical Science, Department of Gastroenterological Surgery
Keio University School of Medicine, Department of Surgery
Kitakyushu Municipal Medical Center, Department of Surgery
Kitasato University School of Medicine, Department of Surgery
Kobe University Graduate School of Medicine, Department of Hepato-Biliary-Pancreatic Surgery
Kumamoto University, Department of Gastroenterological Surgery
Kurume University School of Medicine, Department of Surgery

Kyorin University School of Medicine, Department of Surgery
Kyoto University, Department of Hepato-Biliary-Pancreatic Surgery and Transplantation
Kyushu University, Faculty of Medicine, Department of Surgery I
Matsunami General Hospital, Department of Surgery
Meiwa Hospital, Department of Surgery
Mie University Graduate School of Medicine, Department of Hepatobiliary Pancreatic Surgery
Miyagi Cancer Center, Department of Surgery
Miyazaki University School of Medicine, Department of Surgical Oncology and Regulation of Organ Function
Nagasaki Medical Center, Department of Surgery
Nagasaki University Graduate School of Medicine, Department of Gastroenterological Surgery
Nagasaki University Graduate School of Medicine, Department of Translational Medical Science
Nagoya City University Graduate School of Medical Sciences, Department of Gastroenterological Surgery
Nagoya University Graduate School of Medicine, Department of Gastroenterological Surgery
Nara Medical University, Department of Surgery
National Cancer Center Hospital East, Department of Upper Abdominal Surgery
Nihon University School of Medicine, Division of Digestive Surgery
Niigata Prefectural Central Hospital, Department of Surgery
Niigata University School of Medicine, Department of Surgery
Nippon Medical School, Department of Surgery I
Ogaki Municipal Hopital, Department of Surgery
Okayama University Medical School, Department of Surgery
Osaka City University Graduate School of Medicine, Department of Hepato-Biliary-Pancreatic Surgery
Osaka City University Graduate School of Medicine, Department of Surgical Oncology
Osaka Medical Center for Cancer and Cardiovascular Diseases, Department of Surgery
Osaka University Graduate School of Medicine, Department of Gastroentelogical Surgery
Rinku Medical Center, Department of Surgery
Saku Central Hospital, Department of Surgery
Saga University Faculty of Medicine, Department of Surgery
Sapporo Medical University, Department of Surgery I
Saitama Medical University International Medical Center, Department of Surgery
Shiga University of Medical Science, Department of Surgery
Shinshu University School of Medicine, Department of Surgery
Showa University School of Medicine, Department of Surgery
St. Marianna University School of Medicine, Department of Surgery
St. Marianna University, Yokohama City Seibu Hospital, Department of Surgery
Teikyo University, Department of Surgery
Teikyo University Chiba Medical Center, Department of Surgery
Tochigi Cancer Center, Department of Surgery
Tobata Kyoritsu Hospital, Department of Surgery
Tohoku University Graduate School of Medicine, Department of Surgery, Division of Hepato-Biliary-Pancreatic Surgery
Tokai University, School of Medicine, Department of Gastroenterological Surgery
Tokyo Medical and Dental University, Department of Hepato-Biliary-Pancreatic Surgery
Tokyo Medical and Dental University Ichikawa General Hospital, Department of Surgery
Tokyo Medical University, Department of Surgery
Tokyo Women's Medical University Medical Center East, Department of Surgery
Tokyo Women's Medical University, Institute of Gastroenterology, Department of Gastroenterological Surgery
University of Occupational and Environmental Health, Department of Surgery I
University of Yamanashi Faculty of Medicine, Department of Surgery I
Wakayama Medical University, Second Department of Surgery
Yamagata University Faculty of Medicine, Department of Gastroenterological and General Surgery
Yamaguchi University Graduate School of Medicine, Department of Digestive Surgery and Surgical Oncology
Yame General Hospital, Department of Surgery
Yokohama City University, Department of Gastroenterological Surgery.

REFERENCES

1. Yeo CJ, Cameron JL, Sohn TA, Lillemoe KD, Pitt HA, Talamini MA, et al. Six hundred fifty consecutive pancreaticoduodenectomies in the 1990s: pathology, complications, and outcomes. Ann Surg 1997;226:248-57.
2. Neoptolemos JP, Russell RCG, Bramhall S, Theis B. Low mortality following resection for pancreatic and periampullary tumours in 1026 patients: UK survey of specialist pancreatic units. Br J Surg 1997;84:1370-6.
3. Büchler MW, Friess H, Wagner M, Kulli C, Wagener V, Z'Graggen K. Pancreatic fistula after pancreatic head resection. Br J Surg 2000;87:883-9.

4. Winter JM, Cameron JL, Campbell KA, Arnold MA, Chang DC, Coleman J, et al. 1423 pancreaticoduodenectomies for pancreatic cancer: a single-institution experience. J Gastrointest Surg 2006;10:1199-211.
5. McPhee JT, Hill JS, Whalen GF, Zayaruzny M, Litwin DE, Sullivan ME, et al. Perioperative mortality for pancreatectomy: a national perspective. Ann Surg 2007;246: 246-53.
6. Moriura S, Ikeda S, Ikezawa T, Naiki K. The inclusion of an omental flap in pancreatoduodenectomy. Surg Today 1994; 24:940-1.
7. Fong Y, Gonen M, Rubin D, Radzyner M, Brennan MF. Long-term survival is superior after resection for cancer in high-volume centers. Ann Surg 2005;242:540-4.
8. Hirata K, Sato T, Mukaiya M, Yamashiro K, Kimura M, Sasaki K, et al. Results of 1001 pancreatic resections for invasive ductal adenocarcinoma of the pancreas. Arch Surg 1997; 132:771-6.
9. Imaizumi T, Hanyu F, Harada N, Hatori T, Fukuda A. Extended radical Whipple resection for cancer of the pancreatic head: operative procedure and results. Dig Surg 1998; 15:299-307.
10. Kawai M, Tani M, Terasawa H, Ina S, Hirono S, Nishioka R, et al. Early removal of prophylactic drains reduces the risk of intra-abdominal infections in patients with pancreatic head resection: prospective study for 104 consecutive patients. Ann Surg 2006;244:1-7.
11. Kasuaya H, Nakao A, Nomoto S, Hosono J, Takeda S, Kaneko T, et al. Postoperative delayed emptying in pylorus-preserving pancreatoduodenectomy using pancreaticogastrostomy: comparison of the reconstruction position. Hepatogastroenterology 1997;44:856-60.
12. Tani M, Terasawa H, Kawai M, Ina S, Hirono S, Uchiyama K, et al. Improvement of delayed gastric emptying in pylorus-preserving pancreaticoduodenectomy: results of a prospective, randomized, controlled trial. Ann Surg 2006; 243:316-20.
13. Tani M, Kawai M, Yamaue H. Intraabdominal hemorrhage after a pancreatectomy. J Hepatobiliary Pancreat Surg 2008;15:257-61.
14. Miura F, Asano T, Amano H, Yoshida M, Toyota N, Wada K, et al. Management of postoperative arterial hemorrhage after pancreato-biliary surgery according to the site of bleeding: relaparotomy or interventional radiology. J Hepatobiliary Pancreat Surg 2009;16:56-63.
15. Matsuno S, Egawa S, Fukuyama S, Motoi F, Sunamura M, Isaji S, et al. Pancreatic cancer registry in Japan. Pancreas 2004;28:219-30.
16. Bassi C, Dervenis C, Butturini G, Fingerhut A, Yeo C, Izbicki J, et al. Postoperative pancreatic fistula: an international study group (ISGPF) definition. Surgery 2005;138:8-13.
17. Iannitti DA, Coburn NG, Somberg J, Ryder BA, Monchik J, Cioffi WG. Use of the round ligament of the liver to decrease pancreatic fistulas: a novel technique. J Am Coll Surg 2006;203:857-64.
18. Abe N, Sugiyama M, Suzuki Y, Yanagida O, Masaki T, Mori T, et al. Falciform ligament in pancreatoduodenectomy for protection of skeletonized and divided vessels. J Hepatobiliary Pancreat Surg 2009;16:184-8.
19. Kurosaki I, Hatakeyama K. Omental wrapping of skeletonized major vessels after pancreaticoduodenectomy. Int Surg 2004;89:90-4.
20. Maeda A, Ebata T, Kanemoto H, Matsunaga K, Bando E, Yamaguchi S, et al. Omental flap in pancreaticoduodenectomy for protection of splanchnic vessels. World J Surg 2005;29:1122-6.
21. Wente MN, Bassi C, Dervenis C, Fingerhut A, Gouma DJ, Izbicki JR, et al. Delayed gastric emptying (DGE) after pancreatic surgery: a suggested definition by the International Study Group of Pancreatic Surgery (ISGPS). Surgery 2007;142:761-8.
22. Wente MN, Veit JA, Bassi C, Dervenis C, Fingerhut A, Gouma DJ, et al. Postpancreatectomy hemorrhage (PPH): an International Study Group of Pancreatic Surgery (ISGPS) definition. Surgery 2007;142:20-5.

J Hepatobiliary Pancreat Sci (2012) 19:95–99
DOI 10.1007/s00534-011-0476-4

Pancreatic dissection in the procedure of pancreaticoduodenectomy (with videos)

Hiroki Yamaue · Masaji Tani · Manabu Kawai · Seiko Hirono · Ken-ichi Okada · Motoki Miyazawa

Published online: 11 November 2011

Abstract The procedure of pancreaticoduodenectomy consists of three parts: resection, lymph node dissection, and reconstruction. A transection of the pancreas is commonly performed after a maneuver of the pancreatic head, exposing of the portal vein or lymph node dissection, and it should be confirmed as a safe method for pancreatic transection for decreasing the incidence of pancreatic fistula. However, there are only a few clinical trials with high levels of evidence for pancreatic surgery. In this report, we discuss the following issues: dissection of peripancreatic tissue, exposing the portal vein, pancreatic transection, dissection of the right hemicircle of the peri-superior mesenteric artery including plexus and lymph nodes, and dissection of the pancreatic parenchyma.

Keywords Pancreaticoduodenectomy · Energy device · Pancreatic resection

This article is based on the studies first reported in Highly Advanced Surgery for Hepato-Biliary-Pancreatic Field (in Japanese). Tokyo: Igaku-Shoin, 2010.

Electronic supplementary material The online version of this article (doi:10.1007/s00534-011-0476-4) contains supplementary material, which is available to authorized users.

H. Yamaue (✉) · M. Tani · M. Kawai · S. Hirono · K. Okada · M. Miyazawa
Second Department of Surgery, Wakayama Medical University, Wakayama, Japan
e-mail: yamaue-h@wakayama-med.ac.jp

Introduction

Pancreaticoduodenectomy (PD) is a standard surgery involving pancreatic head resection for periampullary lesions. Persistent complications of PD have been reported which include pancreatic fistula, intra-abdominal abscess, intra-abdominal hemorrhage, and delayed gastric emptying (DGE). Pancreatic fistula is associated with all of these postoperative complications and contributes to overall morbidity and mortality. To reduce the surgical complications, we must develop improved methods of pancreatic dissection and reconstruction. However, there are only a few clinical trials with high levels of evidence for pancreatic surgery. In terms of lymph node dissection, several controlled trials have been performed to date, and extended lymph node dissection is not recommended to improve survival; moreover, the rate of postoperative complications is definitively high in patients with extended surgery [1–3].

One step in improving the survival of pancreatic cancer patients is to perform postoperative chemotherapy immediately after surgery. To begin postoperative chemotherapy as soon as possible after surgery, safe pancreatic surgery is essential. In this chapter, we discuss how to dissect the pancreatic parenchyma safely without postoperative complications.

The procedures of pancreaticoduodenectomy

The procedure of pancreaticoduodenectomy consists of three parts: resection, lymph node dissection, and reconstruction. Resection requires not only a lower volume of intraoperative blood loss for less-invasive surgery, but also the decision of an optimal resection area based on surgical oncology. Reconstruction is important in preventing

postoperative complications, including pancreatic fistula, which is the most dreaded complication of pancreatic surgery. Transection of the pancreas is commonly performed after a maneuver of the pancreatic head, exposing of the portal vein, or lymph node dissection, and it should be confirmed as a safe method for pancreatic transection for decreasing the incidence of pancreatic fistula. In this report, we explain dissection of peripancreatic tissue, exposing the portal vein, pancreatic transection, and dissection of the right hemicircle of the peri-superior mesenteric artery including plexus and lymph nodes.

The recommended technique for pancreaticoduodenectomy uses a midline incision from the xiphoid process to 5 cm under the navel. When an upper view is not enough to perform surgical procedures, the surgical field should be expanded by removal of the xiphoid process. Although a small incision is the recent fashion, a large incision is useful for decreasing the incidence of postoperative complications by means of a wide surgical field. Therefore, pancreaticoduodenectomy follows the rule, "great surgeon makes big incision", and pancreaticoduodenectomy is distinguished from the concept of a function-preserving operation.

The round ligament of the liver and the falciform ligament are divided after laparotomy, and the wide surgical field is maintained through the use af a self-retaining retractor. The embryonic pancreas adheres to retroperitoneum of the posterior abdominal wall, accompanied by the rotation of the embryonic duodenum. The right half of the pancreas consisting of the pancreatic head, pancreatic neck, and a part of pancreatic body, is fixed by the Treiz ligament, which develops by fusing the dorsal surface of the pancreas into the parietal peritoneum. The Kocher maneuver is the remobilization of the pancreatic head by dissection.

The Kocher maneuver is begun at the third portion of the duodenum to the right edge of the hepatoduodenal ligament, and it continues to left renal vein (Fig. 1). This procedure eases identification of the origin of the proximal superior mesenteric artery (SMA). First, the pancreatic head plexus is dissected. At this time, it is possible to tape the SMA, however, it is not always necessary do so. Although the proximal celiac trunk is also identified coincidentally, we do not perform routine taping.

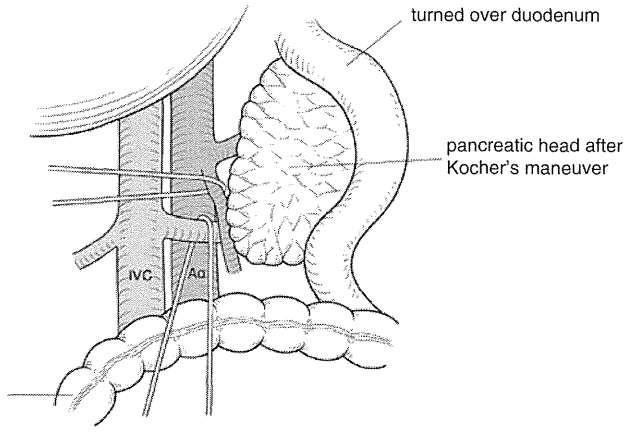

Fig. 1 Kocher maneuver. The Kocher maneuver is promoted to the right edge of hepatoduodenal ligament. Extended resection is performed to dissect the plexus and tissue surrounding the SMA. Taping of the SMA is not essential at this time. *Ao* aorta, *IVC* inferior vena cava

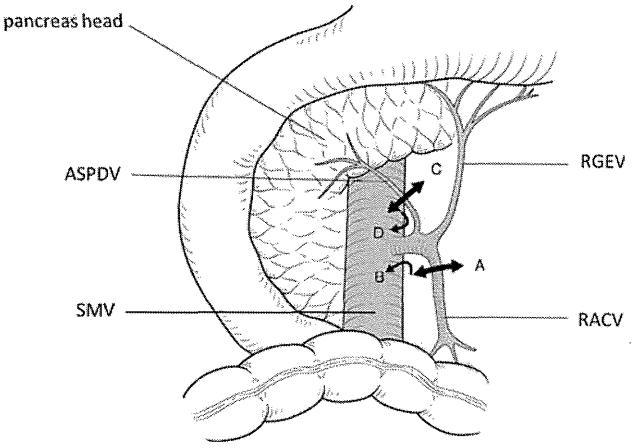

Fig. 2 Manipulation of gastrocolic trunk. For beginners, it is difficult to manipulate the gastrocolic trunk (GCT). First, the right accessory colic vein is divided (*A*), and the lower side of the GCT is dissected (*B*). Next, it is easy to identify the neck of GCT following the division of the anterior superior pancreaticoduodenal vein (*C*) and dissection of upper side of the GCT (*D*). Division of the GCT makes it easy to expose the superior mesenteric vein. *ASPDV* anterior superior pancreatoduodenal vein, *RGEV* right gastroepiploic vein, *RACV* right accessory colic vein

Dissection around the portal vein and tunneling behind the pancreas neck

In the next step, a tunnel is created between the anterior surface of the portal vein (PV) and the pancreas neck. The ascending and transverse mesocolon fuses to the anterior leaf of the mesoduodenum at a level just above the pancreatic head. This fusion is an extension of the right Toldt fusion fascia, which is formed by the fusion between the ascending mesocolon and parietal peritoneum. The superior mesenteric vein (SMV) trunk can be identified when the transverse colon is dissected from the duodenum between the anterior leaves of the transverse mesocolon and the mesoduodenum. In a case with portal vein invasion, the branch vein of the PV-SMV system is often enhanced. Therefore, it is necessary to ligate the branch vein carefully when the gastrocolic trunk root is ligated. The accessory right colic vein and anterior superior pancreaticoduodenal vein (ASPDV) should be divided first before the gastrocolic trunk of Henle is divided (Fig. 2). By

this method, the operative field develops, and the gastrocolic trunk of Henle can be easily identified, even by a beginner. Because this scene of tunneling between the anterior surface of the portal vein and the pancreas neck bleeds easily, it is necessary to ligate the gastrocolic trunk first.

In a case of invasion of the front side of the PV, tunneling between the anterior surface of the PV and the pancreas neck is impossible. However, in a case with invasion only of the right or left side of the PV, tunneling from the other side is possible.

Unexpected bleeding may be caused when the PV is dissected. It is possible to stop bleeding reliably even at such a time as follows: the portal vein pressure is basically low. PV pressure returns to a low level when you hold the pancreas in its former position without panicking. By that means, the portal vein pressure should be prevented from going up. The bleeding point is usually a pin-point hole but not a fissure. when the bleeding point is not a split but only a pin-point hole, pressure by one finger can stop the bleeding. If you panic and clamp the vessel with forceps or blindly suture it, the fissure will get larger. In this case, hemostasis is already difficult, and you will have to cope with a large amount of bleeding. Do not hold the vessel, but press with one finger or fine forceps. In this way, the amount of bleeding is reduced. Adequate suture by unabsorbable monofilament will stop bleeding. Techniques to stop bleeding from the portal vein system are essential when performing PD.

Lymph node dissection of the region around the common hepatic artery from hepatoduodenal ligament

After tunneling, you can perform omentectomy using ultrasonic coagulating devices. The right gastroepiploic artery is ligated, and then No6 lymph node dissection is performed [1]. Gastrectomy is performed at a 1–2 cm oral line from the pylorus ring, in order to preserve the distal gastric blood supply for prevention of delayed gastric emptying.

Next, gastroduodenal artery taping is performed, followed by proper hepatic artery taping. At this time, it is important to identify and tape the right hepatic artery to avoid damage of the right hepatic artery during dissection around the bile duct; carefully review the video for this important maneuver.

After cholecystectomy, the bile duct is cut at the level of the common hepatic duct, and the margin of the bile duct is pathologically diagnosed to determine whether cancer cells are present. The hepatic cutting margin of the bile duct is clamped with blood vessel forceps to prevent leakage of bile juice, while the proximal margin of the bile duct is transfixed ligated. No12a, b, p lymph node dissection is performed while checking the portal vein back face, and the No12 lymph node is connected with the dissected No8 lymph node, then the No12 and No8 lymph node dissection is done together [2, 3]. After that, dual ligation of the gastroduodenal artery is performed, and you can find the exposed portal vein trunk.

Pancreatic resection and duodenal resection

Before pancreatic resection, we routinely prepare the pancreas to cut back on blood loss from bilateral pancreatic cut ends. We tie the duodenal side with 2-0 bladed silk, and fasten the distal side gently with a vessel loop to control bleeding from the inferior pancreatic artery. Clamping of the distal pancreas should be performed gently, so as not to crush the pancreatic parenchyma. A No11 scalpel blade is usually used in resection of the pancreas, and frozen sections of the whole pancreatic cut end margin are produced. Sharp and fast resection by scalpel blade is fine, and it is easy to recognize the narrow pancreatic duct compared with a blunt dissection. After complete hemostasis, a 2–3 mm tube is inserted to confirm the patency and direction of the pancreatic duct (Fig. 3).

As regards the pancreatic resection, there are several ways, reported as follows; (1) resecting the pancreas sharply with a scalpel blade, (2) using electric cautery, (3)

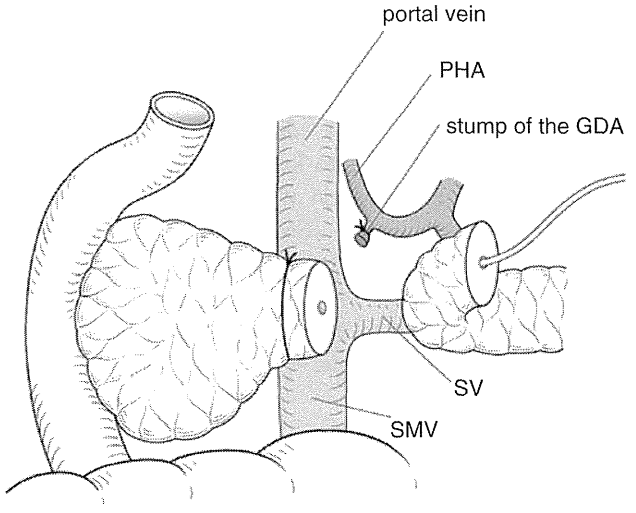

Fig. 3 Transection of the pancreas. The pancreas is sharply transected with a knife on the left edge of the portal vein. Minute hemorrhage from the surgical stump of the remnant pancreas was stopped by electrosurgical devices, and only the arterial hemorrhage was ligated by 5-0 prolene. Preserving the blood stream of the surgical stump of the remnant pancreas is important to prevent pancreatic fistula. *PHA* proper hepatic artery, *GDA* gastroduodenal artery, *SV* splenic vein, *SMV* superior mesenteric vein

clamping the micropancreatic duct after clamping parenchyma by CUSA® or forceps, (4) using bipolar scissors, (5) using a diathermy knife (The LigaSure™ vessel sealing system or Harmonic scalpel®).

1. Pancreatic resection by scalpel blade is the simplest way and does not take much time. The cut end surface is smooth and does not damage blood perfusion on the pancreatic cut end. Just after resection, the surgeon often encounters active bleeding from inferior pancreatic arteries, which should be managed by transfixing suture closure of 5-0 prolene. The hemostasis of oozing blood from the cut end is easy (video 1).
2. Electric cautery is good at control bleeding, but the surgeon should take care to avoid damage of the cut end perfusion by deep coagulation effect.
3. Clamping is another method by ligation of the micropancreatic duct to prevent pancreatic fistula. It requires time compared with othermethods, and it is actually impossible to entirely ligate the pancreatic duct and to completely prevent pancreatic fistula.
4. The Harmonic scalpel® and LigaSure™ vessel sealing system are excellent at hemostasis and have narrow coagulation fields, but there is a possibility this approach might seal the small pancreatic duct, causing it to lose itself in the cut surface (video 2).

There are advantages and disadvantages to each procedure or device in pancreatic resection. The real value of each method in preventing pancreatic fistula needs to be confirmed in large-scale clinical studies.

The dissection of the nerve plexus around the superior mesenteric artery

When SMV and the portal vein (SMPV) are taped at two points and pulled to the left by vascular tapes, the pulsation of the SMA is palpated directly under the SMPV. Anatomically, the SMA travels from the left side to run along with SMV; it is easier to confirm the pulsation at the distal position than proximal position (Fig. 4). The anterior aspect of the nerve plexus around the SMA is divided by Kelly forceps, and the second portion of the right nerve plexus around the SMA is resected (Fig. 4). Basically, left nerve plexus around the SMA is preserved. The knack of decreasing intraoperative blood loss is to ligate and to divide the inferior pancreaticoduodenal artery (IPDA) as early as possible [4, 5]. It is useful and recommended to determine the location of the IPDA branch point from the SMA by preoperative CT-angiography [6]. After the the first and second portion of right plexus is dissected, the SMA branch point from the aorta is exposed and the right celiac ganglion can be dissected. The dissection of the right nerve plexus around the SMA and the right celiac ganglion goes smoothly by using the vascular tape, which was previously taped at the SMA branch point from the aorta via the Kocher maneuver, as a guide.

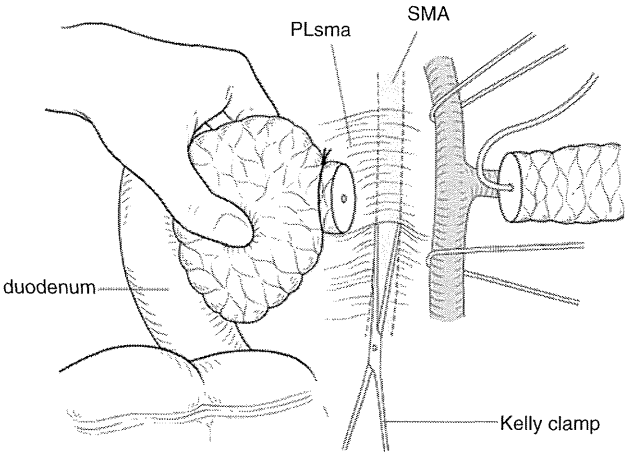

Fig. 4 Dissection of nerve plexuses of the superior mesenteric artery (SMA) The connective tissue and nerve plexuses of SMA were dissected on the SMA. The inferior pancreatoduedenal artery (IPDA) should be detected and ligated promptly to reduce intraoperative bleeding. *PLsma* plexuses of superior mesenteric artery

Dos & don'ts

1. During tunneling procedures, dissection and dividing of the upper edge of the pancreas should be performed completely, and the branches of portal vein ligated gently and divided.
2. Dissection of the pancreas should be done by gentle methods to avoid pancreatic detrition.
3. Dissection of the pancreatic remnant should be limited to safely performing anastomosis.

Discussion

Pancreatic resection has become safer by using new surgical devices to control blood loss. However, pancreatic resection using surgical devices has both advantages and disadvantages [6]. It is important to develop surgical techniques of pancreatic resection to prevent postoperative morbidities such as pancreatic fistula [7]. Various methods and techniques for treating the dissection of the pancreatic parenchyma have been reported to reduce pancreatic fistula after PD. Appropriate surgical stump closure after PD is still controversial. Bipolar scissors (Ethicon Endo-Surgery, Cincinnati, OH, USA) is a device that combines cutting with coagulation, and current crosses only between the two

forceps of the electrode. This instrument has the characteristic of less thermal injury of the cut surface and better hemostasis. We conducted a clinical trial using this device to determine whether the rate of pancreatic fistula is reduced in patients with distal pancreatectomy [8]. For the present, we are proceeding to dissect the pancreatic parenchyma using the new energy device Harmonic-Scalpel (Ethicon Endo-Surgery), and have had a better result in terms of the rate of pancreatic fistula in patients with pancreatic head resection. However, this study has several limitations, including retrospective data collection. Therefore, a randomized controlled trial is needed to achieve the final answer as to which procedure ibest for dissecting the pancreatic parenchyma.

Critical and important points

1. The critical point of pancreaticoduodenectomy is tunneling between the portal vein and pancreatic parenchyma of the neck, and this procedure is essential for pancreaticoduodenectomy.
2. It is important to understand of the anatomy of the gastrocolic trunk when tunneling.
3. The preservation of blood supply in the resecting surface of the pancreas is essential for prevention of postoperative complications, including pancreatic fistula.
4. The gentle management of the cutting edge of the pancreas is critical for prevention of postoperative pancreatic fistula.

Conflict of interest The authors declare that they have no conflict of interest.

References

1. Yeo CJ, Cameron JL, Lillemoe KD, et al. Pancreaticoduodenectomy with or without distal gastrectomy and extended retroperitoneal lymphadenectomy for periampullary adenocarcinoma, part 2: randomized controlled trial evaluating survival, morbidity, and mortality. Ann Surg. 2002;236:355–66.
2. Raut CP, Tseng JF, Sun CC, et al. Impact of resection status on pattern of failure and survival after pancreaticoduodenectomy for pancreatic adenocarcinoma. Ann Surg. 2007;246:52–60.
3. Pedrazzoli S, Dionigi R, Mosca F, et al. Standard versus extended lymphadenectomy associated with pancreatoduodenectomy in the surgical treatment of adenocarcinoma of the head of the pancreas: a multicenter, prospective, randomized study. Lymphadenectomy Study Group. Ann Surg. 1998;228:508–17.
4. Ohigashi H, Ishikawa O, Eguchi H, et al. Early ligation of the inferior pancreaticoduodenal artery to reduce blood loss during pancreaticoduodenectomy. Hepatogastroenterology. 2004;51:4–5.
5. Ishizaki Y, Sugo H, Yoshimoto J, et al. Pancreatoduodenectomy with or without early ligation of the inferior pancreatoduodenal artery: comparison of intraoperative blood loss and short-term outcome. World J Surg. 2010;34:2939–44.
6. Kawai M, Tani M, Ina S, et al. CLIP method (preoperative CT image-assessed ligation of inferior pancreaticoduodenal artery) reduces intraoperative bleeding during pancreaticoduodenectomy. World J Surg. 2008;32:82–7.
7. Suc B, Msika S, Fingerhut A, et al. Temporary fibrin glue occlusion of the main pancreatic duct in the prevention of intra-abdominal complications after pancreatic resection: prospective randomized trial. Ann Surg. 2003;237:57–65.
8. Kawai M, Tani M, Yamaue H. Transection using bipolar scissors reduces pancreatic fistula after distal pancreatectomy. J Hepatobiliary Pancreat Surg. 2008;15:861–4.

Whole-exome sequencing of human pancreatic cancers and characterization of genomic instability caused by *MLH1* haploinsufficiency and complete deficiency

Linghua Wang,[1] Shuichi Tsutsumi,[1] Tokuichi Kawaguchi,[2] Koichi Nagasaki,[3] Kenji Tatsuno,[1] Shogo Yamamoto,[1] Fei Sang,[1] Kohtaro Sonoda,[1] Minoru Sugawara,[3] Akio Saiura,[4] Seiko Hirono,[5] Hiroki Yamaue,[5] Yoshio Miki,[3,6] Minoru Isomura,[3] Yasushi Totoki,[7] Genta Nagae,[1] Takayuki Isagawa,[1] Hiroki Ueda,[1] Satsuki Murayama-Hosokawa,[8] Tatsuhiro Shibata,[7] Hiromi Sakamoto,[9] Yae Kanai,[10] Atsushi Kaneda,[1] Tetsuo Noda,[3] and Hiroyuki Aburatani[1,11]

[1]*Genome Science Division, Research Center for Advanced Science and Technology (RCAST), The University of Tokyo, Tokyo 153-8904, Japan;* [2]*Department of Cell Biology, Cancer Institute, Japanese Foundation for Cancer Research (JFCR), Tokyo 135-8550, Japan;* [3]*Genome Center, Cancer Institute, Japanese Foundation for Cancer Research (JFCR), Tokyo 135-8550, Japan;* [4]*Department of Gastroenterological Surgery, Cancer Institute Hospital, Japanese Foundation for Cancer Research (JFCR), Tokyo 135-8550, Japan;* [5]*Second Department of Surgery, Wakayama Medical University School of Medicine, Wakayama 641-8510, Japan;* [6]*Department of Molecular Genetics, Medical Research Institute, Tokyo Medical and Dental University, Tokyo 113-8510, Japan;* [7]*Division of Cancer Genomics, National Cancer Center Research Institute, Tokyo 104-0045, Japan;* [8]*Department of Obstetrics and Gynecology, Faculty of Medicine, The University of Tokyo, Tokyo 113-8655, Japan;* [9]*Division of Genetics, National Cancer Center Research Institute, Tokyo 104-0045, Japan;* [10]*Division of Molecular Pathology, National Cancer Center Research Institute, Tokyo 104-0045, Japan*

Whole-exome sequencing (Exome-seq) has been successfully applied in several recent studies. We here sequenced the exomes of 15 pancreatic tumor cell lines and their matched normal samples. We captured 162,073 exons of 16,954 genes and sequenced the targeted regions to a mean coverage of 56-fold. This study identified a total of 1517 somatic mutations and validated 934 mutations by transcriptome sequencing. We detected recurrent mutations in 56 genes. Among them, 41 have not been described. The mutation rates varied widely among cell lines. The diversity of the mutation rates was significantly correlated with the distinct *MLH1* copy-number status. Exome-seq revealed intensive genomic instability in a cell line with *MLH1* homozygous deletion, indicated by a dramatically elevated rate of somatic substitutions, small insertions/deletions (indels), as well as indels in microsatellites. Notably, we found that *MLH1* expression was decreased by nearly half in cell lines with an allelic loss of *MLH1*. While these cell lines were negative in conventional microsatellite instability assay, they showed a 10.5-fold increase in the rate of somatic indels, e.g., truncating indels in *TP53* and *TGFBR2*, indicating *MLH1* haploinsufficiency in the correction of DNA indel errors. We further analyzed the exomes of 15 renal cell carcinomas and confirmed *MLH1* haploinsufficiency. We observed a much higher rate of indel mutations in the affected cases and identified recurrent truncating indels in several cancer genes such as *VHL*, *PBRM1*, and *JARID1C*. Together, our data suggest that *MLH1* hemizygous deletion, through increasing the rate of indel mutations, could drive the development and progression of sporadic cancers.

[Supplemental material is available for this article.]

The current understanding of cancer is that it arises as a result of the accumulation of genetic and epigenetic mutations that confer a selective advantage to the cells in which they occur (Vogelstein and Kinzler 2004; Greenman et al. 2007; Stratton et al. 2009). Over the past quarter of a century, many efforts have been made to learn about the causative mutations that drive various types of cancer, including pancreatic cancer, one of the most lethal forms of human cancer. By using the Sanger sequencing method, i.e., PCR amplification followed by plasmid subcloning and DNA sequencing, previous studies have identified thousands of genetic alterations in the cancer genome and provided important insights into the pancreatic cancer biology (Jones et al. 2008; Maitra and Hruban 2008). However, because Sanger sequencing is performed on single amplicons, its throughput is limited, and large-scale sequencing projects are expensive and laborious (Schuster 2008; Metzker 2010). Moreover, it has been reported that it has a limited sensitivity to recognize the mutant DNA allele if it is present in a minor population of cancer cells (Nakahori et al. 1995; Thomas et al. 2006; Qiu et al. 2008). In addition, the bacterial cloning workflows tend to be complex and time-consuming, and bias can be introduced into this step (Thomas et al. 2006).

The advent of next-generation sequencing (NGS) technologies has brought a high level of efficiency to genome sequencing (Schuster 2008; Metzker 2010). The enriched DNA is sequenced directly, avoiding the cloning step (Ng et al. 2009). While whole-genome

[11]Corresponding author.
E-mail haburata-tky@umin.ac.jp.
Article published online before print. Article, supplemental material, and publication date are at http://www.genome.org/cgi/doi/10.1101/gr.123109.111.

22:208–219 © 2012 by Cold Spring Harbor Laboratory Press; ISSN 1088-9051/12; www.genome.org

sequencing is the most complete, it remains sufficiently expensive that cost-effective alternatives are important. Target-enrichment strategies allow the selective capture of the genomic regions of interest. Whole-exome sequencing (Exome-seq) through integrating two systems has enabled us to concentrate our sequencing efforts on the protein-coding exons in the human genome. This approach is substantially cost- and labor-efficient (Schuster 2008; Metzker 2010; Biesecker et al. 2011). Moreover, by taking advantage of deep coverage of target regions, it shows an excellent sensitivity for the detection of variants with a minor allele frequency down to 2% (Li et al. 2010). Recent studies have successfully applied Exome-seq to identify genetic changes involved in Mendelian diseases (Choi et al. 2009; Ng et al. 2010). In addition to Exome-seq, full-length transcriptome sequencing (mRNA-seq) offers a fast and inexpensive alternative. It is an easier method to identify coding sequences and capture variants in genes that are expressed, as well as to generate additional information, such as gene expression level and splicing patterns (Sugarbaker et al. 2008; Cirulli et al. 2010).

Genomic instability is a characteristic feature of almost all human cancers (Lengauer et al. 1998; Negrini et al. 2010). Its molecular basis is well understood in hereditary cancers, in which it has been linked to mutations in DNA mismatch repair (MMR) genes. One of the best-documented examples is the hereditary nonpolyposis colon cancer (HNPCC). In general, MMR defects are the result of a germline mutation in one of the MMR genes followed by a hit on the second allele of that gene, or methylation of the promoter of a MMR gene, usually *MLH1*, resulting in the loss of protein function (Fishel et al. 1993; Hemminki et al. 1994). In contrast, the molecular basis of genomic instability in sporadic cancers remains unclear (Negrini et al. 2010).

In the past few years, by use of Sanger sequencing, several consortia have scanned the coding sequences of 18,191–20,661 genes in carcinomas of the colon, breast, and pancreas and in glioblastomas (Sjoblom et al. 2006; Wood et al. 2007; Jones et al. 2008; Parsons et al. 2008). These genome-wide studies reported that mutations targeting caretaker genes (DNA repair genes and mitotic checkpoint genes) were infrequent. To date, no statistical correlation has been described in sporadic cancers between the allelic loss of a caretaker gene and the increased rate of genomic instability. It has been thought that a single copy of the wild-type allele of a caretaker gene is sufficient to perform its normal function, and both alleles of the gene would have to be inactivated before the genome becomes unstable (Bodmer et al. 2008; Negrini et al. 2010). Since the occurrence of two independent somatic mutations at both alleles of the same gene is likely to represent a very rare event (Bodmer et al. 2008), these studies argued that mutations in caretaker genes probably do not account for the presence of genomic instability in many sporadic cancers (Negrini et al. 2010).

We here performed Exome-seq on 15 pancreatic ductal adenocarcinoma (PDAC)–derived cell lines. This study identified 1517 somatic mutations and validated 934 of them by mRNA-seq. We notably found a significant correlation between *MLH1* allelic loss and the increased rate of somatic indel mutations, and we further confirmed this finding in primary renal cell carcinomas (RCCs). In the affected cases, we detected recurrent truncating indels that inactivate tumor suppressor genes, such as *TP53*, *TGFBR2*, and *VHL*. We also observed a higher prevalence of indels in the coding microsatellite sequences. Our data, therefore, indicate that deletion of one copy of the *MLH1* gene results in haploinsufficiency in the correction of DNA indel errors and could be a driving force in pancreatic and renal carcinogenesis.

Results

The performance of Exome-seq

We sequenced the exomes of 15 PDAC-derived cell lines and their matched normal samples (Table 1). On average, 6.6 Gb of high-quality sequence data (about 44.2 million paired 75-base reads) were generated per sample. More than 88% of the sequence reads were uniquely aligned to the human reference genome with the expected insert size and correct orientations, and 68.4% of them fell within the targeted regions (Fig. 1A; Supplemental Fig. S1). The average fold-coverage of each exome was 56× (Supplemental Fig. S2). On average per exome, 96.9% of targeted bases were covered by at least one read, and 83.4% of targeted bases were covered by at least 10 reads (Fig. 1B; Supplemental Fig. S3).

An overview of somatic mutations

By using Exome-seq, we identified a total of 1517 somatic mutations, including 39 nonsense, 833 missense, 423 synonymous substitutions, and 49 substitutions in untranslated regions (UTRs), 137 frame-shift indels and 36 in-frame indels (Fig. 1C). The complete list

Table 1. *Characteristics of pancreatic tumor cell lines*

Sample OID	Carcinoma type	Pathology	Differentiation	Lymph node metastasis	Tissue derivation	Sample type	*MLH1* status
PA018	Ductal adenocarcinoma	Tubular	Moderately	–	Primary pancreatic tumor	Cell line	LOH
PA028	Ductal adenocarcinoma	Tubular	Moderately	+	Primary pancreatic tumor	Cell line	ROH
PA055	Ductal adenocarcinoma	Tubular	Moderately	+	Primary pancreatic tumor	Cell line	LOH
PA086	Ductal adenocarcinoma	Tubular	Moderately	+	Primary pancreatic tumor	Cell line	ROH
PA090	Ductal adenocarcinoma	Tubular	Well	+	Primary pancreatic tumor	Cell line	ROH
PA107	Ductal adenocarcinoma	Invasive	Moderately to well	–	Primary pancreatic tumor	Cell line	ROH
PA122	Ductal adenocarcinoma	Invasive	Moderately to poorly	–	Primary pancreatic tumor	Cell line	ROH
PA167	Ductal adenocarcinoma	Invasive	Moderately	+	Primary pancreatic tumor	Cell line	LOH
PA182	Ductal adenocarcinoma	Invasive	Moderately	+	Primary pancreatic tumor	Cell line	ROH
PA195	Ductal adenocarcinoma	Tubular	Moderately	+	Primary pancreatic tumor	Cell line	ROH
PA202	Ductal adenocarcinoma	Tubular	Moderately	+	Primary pancreatic tumor	Cell line	LOH
PA215	Ductal adenocarcinoma	Tubular	Poorly	+	Primary pancreatic tumor	Cell line	ROH
PA254	Ductal adenocarcinoma	Tubular	Moderately	–	Primary pancreatic tumor	Cell line	ROH
PA285	Ductal adenocarcinoma	Invasive	Moderately	–	Primary pancreatic tumor	Cell line	HD
PA333	Ductal adenocarcinoma	Tubular	Well	+	Primary pancreatic tumor	Cell line	ROH

ROH indicates retention of heterozygosity; LOH, loss of heterozygosity; and HD, homozygous deletion.

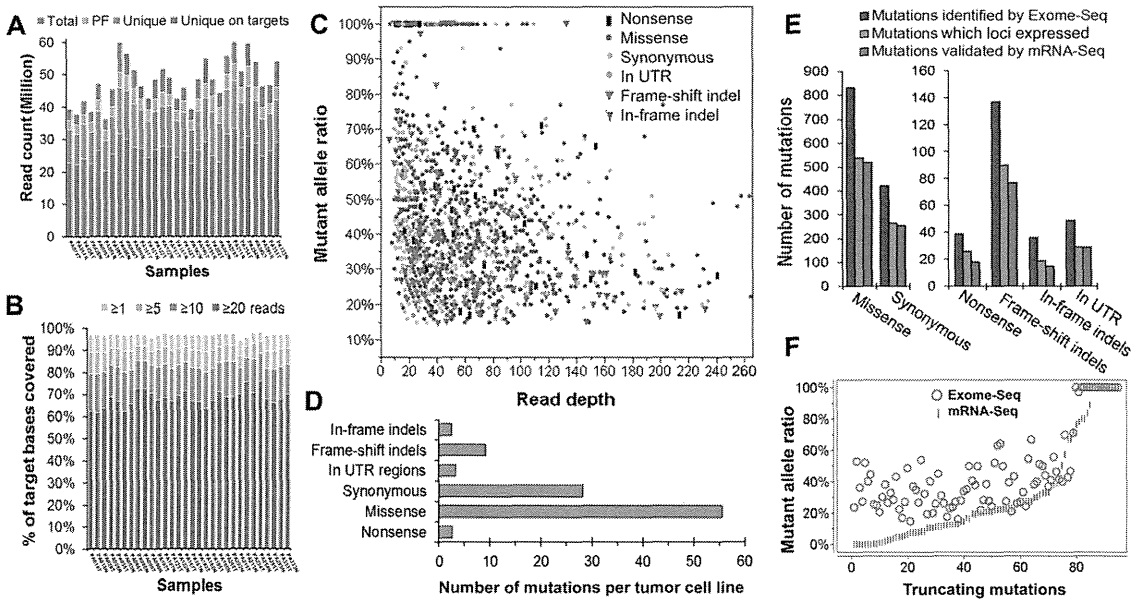

Figure 1. The performance of Exome-seq and a summary of somatic mutations. (*A*) The summary of Exome-seq data. For each sample, the number of raw sequence reads (total), passing filter reads (PF), unique reads that mapped in consistent read pairs (unique), and the unique reads that fall within the targeted regions (unique on target) are shown. (*B*) The sequence coverage of targeted bases. The fraction of the targeted bases that were covered by unique reads at the sequence depth of 1×, 5×, 10×, and 20× is shown. (C) An overview of the somatic mutations identified by Exome-seq. Different markers and colors were used to show different mutation types. (*D*) The average number of somatic mutations identified per tumor cell line. (*E*) The performance of mRNA-seq in verification of somatic mutations identified by Exome-seq. The mutations that loci expressed represent those mutations that loci covered by five or more cDNA sequence reads. (*F*) Validation of the truncating mutations that introduced premature termination codons. The abundance of the mutant alleles in genomic DNA was compared with that of their corresponding cDNA.

of 1517 somatic mutations is shown in Supplemental Table S1. On average, each cell line contains 101 somatic mutations, 89% of which are base substitutions (Fig. 1D). The frequencies of mutant alleles ranged from 15%–100%, with a median of 41%. The depth of coverage at the mutation loci ranged from 10× to 637×, with a median of 42× (Fig. 1C; Supplemental Table S1). The lengths of somatic small indels varied from 1–29 bp. Seventy-eight percent of the indels were 1–3 bp in length (Supplemental Fig. S4). By using genome-wide SNP array, we identified more than 50 focal homozygous deletions (Supplemental Table S2). The *CDKN2A* locus at *9p21.3* and the *SMAD4* locus at *18q21.2* were frequently deleted in the tumor cell lines analyzed (Supplemental Fig. S5). The somatic mutations mainly clustered in nine signaling pathways, as shown in Supplemental Figure S6A. The background mutation rate estimated for targeted exonic regions was 2.7 mutations per megabase of DNA sequences.

Validation of somatic mutations using mRNA-seq

In total, 61.6% (934 out of 1517) of the mutations identified by Exome-seq were validated by mRNA-seq. If we focus on the expressed genes, 94.3% (914 out of 969) of the mutations at those loci covered by five or more cDNA sequence reads were successfully validated by mRNA-seq (Fig. 1E). Additionally, 20 mutations at the loci with a lower coverage (less than five reads, but three reads or more) were also confirmed by mRNA-seq. The percentages of mutations validated by mRNA-seq varied across mutation types. Generally, the validation ratio of truncating mutations is lower than that of nontruncating mutations.

For truncating mutations (Fig. 1F), the abundance of the mutant allele in the cDNA appears to be relatively lower than that of their corresponding genomic DNA (gDNA). Despite the lower abundance, mRNA-seq was still able to confirm 81 of those 94 (86.2%) truncating mutations at loci covered by five or more cDNA sequence reads. The remaining 13 truncating mutations were all heterozygous. Their loci were covered moderately well, but no mutant alleles were observed in the cDNA sequences. We performed Sanger sequencing to confirm if they resulted from the false-positive events of Exome-seq. As shown in Supplemental Figure S7, 12 of the 13 truncating mutations were successfully validated by Sanger sequencing. The mutant alleles were only detected in the gDNA of the tumor cell lines rather than in their cDNA, suggesting the transcripts carrying the mutant alleles were probably degraded through the nonsense-mediated mRNA decay (NMD) pathway (Holbrook et al. 2004). One mutation was found to be false-positive, possibly caused by mapping errors.

The recurrently mutated genes

In this study, 1359 genes were identified with somatic mutations. Among them, 56 genes were recurrently mutated in two or more cell lines (Table 2). The mutation rate of these genes was much higher than the background level. The most frequently mutated gene was *KRAS*, followed by *CDKN2A*, *TP53*, and *SMAD4*. Mutation of these four genes and 11 other genes has been reported either in the COSMIC database (http://www.sanger.ac.uk/genetics/CGP/cosmic/) or in a previous study (Jones et al. 2008), as shown in Supplemental Figure S8, while mutation of the remaining 41 genes, to our knowledge, has not been described in PDAC. Totally, 150 point mutations were identified in the 56 recurrently mutated genes. Among them, 109 mutations in 40 genes were confirmed by mRNA-seq (Supplemental Table S1). For the remaining 41 mutations that were not confirmed by mRNA-seq, seven loci were poorly expressed (covered by two or fewer cDNA sequence reads) and 34 loci were not expressed at all.

Table 2. The recurrently mutated genes

Rank	#Gene symbol	Coding sequence length (bases)	Number of point mutations	Number of DNA copy number variants	Number of deleterious mutations	Normalized mutation rate (mutions/Mb)	Tumor cell lines: PA028T	PA086T	PA090T	PA107T	PA122T	PA182T	PA195T	PA215T	PA254T	PA333T	PA018T	PA055T	PA167T	PA202T	PA285T
1	*KRAS*	570	16	7	**15**	1754.4	S		L	A				A			A	A	A	L	
2	*CDKN2A*	471	1	12	**10**	1415.4		L	P		L						L				
3	*TP53*	1182	12	14	**12**	676.8	L	L		L	L	L	L	L	L	L	L	L	L	L	L
4	*SMAD4*	1659	4	11	**8**	321.5	L					L	L	L	L	L					L
5	***PDCD6***	576	2	4	2	231.5	A							A	A				A		
6	***IL1B***	810	2	1	2	164.6													A		
7	***FAM92B***	915	2	3	2	145.7	A							L					A		
8	*OR4L1*	939	2	3	2	142.0				L		L				L					
9	***SFXN4***	1014	3	1	2	131.5						L									U
10	***RNF207***	1905	3	2	**3**	105.0	L		L												
11	***ASL***	1395	2	1	2	95.6	A														
12	***TYSND1***	1701	2	2	2	78.4					L				L						
13	***ACSM1***	1734	2	3	2	76.9	L							L					A		
14	***NFE2L2***	1818	2	1	2	73.3													A		
15	*PTPRD*	5739	3	14	**6**	69.7	P	L	L	P	L	L	L		P	L	L	L	P	L	SL
16	***CCDC41***	2106	2	6	2	63.3			L	L			L	L			L	L			
17	***EXOC8***	2178	2	-	2	61.2															
18	***CLCN4***	2283	2	3	2	58.4	L							L						L	
19	*KIAA1751*	2289	2	1	2	58.2			L												
20	***SOX5***	2292	2	5	2	58.2				A			A	A				A	A		
21	***WDR75***	2493	2	-	2	53.5															
22	***SAGE1***	2715	2	4	2	49.1	L			L								L		L	
23	*GRM8*	2727	2	2	2	48.9					L			L							
24	***TMTC3***	2745	2	8	2	48.6			L	L	L		L	L		L	L	L			
25	***CNTNAP1***	4155	4	3	**3**	48.1				L			L						L		
26	***ABCC5***	4314	3	1	**3**	46.4				M			A								
27	***CARD10***	3099	3	5	2	43.0	L			L									L	L	ML
28	***PEAR1***	3114	2	-	2	42.8															
29	***FUK***	3255	2	2	2	41.0												L	A		
30	***SORCS1***	3597	2	6	2	37.1					L	L	L		L		L	L			
31	***GIGYF2***	3963	2	1	2	33.6			L												
32	*CNTNAP2*	3996	2	1	2	33.4															
33	***CLIP1***	4284	2	5	2	31.1			L	L				L			L	L			
34	***MYOM3***	4314	2	3	2	30.9	L		L	L											
35	***LPHN1***	4425	2	4	2	30.1	L			L				L				L			
36	***CDC42BPB***	5136	3	3	2	26.0						L	A			L					S
37	***AKAP11***	5706	2	6	2	23.4	L					A		L			L	L	L		
38	***MYH4***	5820	2	10	2	22.9	L	L				L	L	L		L	L	L	L	L	
39	***EXPH5***	5970	2	1	2	22.3						L									
40	***PHF3***	6120	2	3	2	21.8	L											L	L		
41	***CDC42BPG***	6597	2	4	2	20.2		L		L							A		L		
42	*ARID1A*	6858	2	4	2	19.4	L		L	L						L					
43	***SON***	7281	2	2	2	18.3								L				L			
44	*MLL3*	14736	4	5	**4**	18.1	A				L			L				L	L		
45	***IGF2R***	7476	2	6	2	17.8	L						L		L		L	L		L	
46	***IGSF10***	7872	2	2	2	16.9							A				A				
47	***UTP20***	8358	2	6	2	16.0			L	L	L		L	L				L			
48	*VWF*	8442	4	4	2	15.8				A			A				A	A			S
49	***AKAP13***	8454	2	1	2	15.8												L			
50	*BRCA2*	10257	3	4	2	13.0	L							L			L	L	L		
51	*ALMS1*	12504	2	1	2	10.7							A								
52	***FAT2***	13050	2	2	2	10.2							L								L
53	***USH2A***	15609	2	1	2	8.5											L				
54	***MACF1***	16293	2	-	2	8.2															
55	***HMCN1***	16908	2	-	2	7.9															
56	*DNAH9*	17896	2	9	2	7.5	L	L				L	L	L		L	L	L			L

#Gene symbol, the genes colored in orange indicate those genes in which mutations have been described previously in PDAC.

Missense Nonsense Synonymous Frame-shift indel

Homozygous deletion (the entire gene) P: Homozygous deletion (part of the gene)

L: LOH A: Amplification M: +1 Missense S: +1 Synonymous U: +1 substitution in UTR

The widely varied mutation rates

Exome-seq revealed that the mutation rates varied significantly among cell lines (Figs. 2C, 3A). The number of somatic substitutions identified from each cell line ranged from 31–640, and the number of somatic indels varied from zero to 100. Accordingly, we classified the cell lines into three subgroups. Cell lines in group 1 ($n = 10$) showed a modest level of somatic mutations, while cell lines in group 2 ($n = 4$) showed a significantly elevated rate of small indels ($P = 0.005$) (Fig. 2C); a cell line in group 3 ($n = 1$) showed dramatically increased rates of both indels and substitutions (Figs. 2C, 3A). In the group-3 cell line, we observed a much higher prevalence of mutations involved in all nine core signaling pathways ($P = 0.0007$) (Supplemental Fig. S6B). In group-2 cell lines, the normalized mutation rate was slightly but significantly increased ($P = 0.037$) in seven of the nine pathways.

Allelic loss of *MLH1* and the increased mutation rate

To find out the genetic factors that accounted for the increased mutation rate in the group-2 and group-3 cell lines, we first screened the MMR genes for somatic alterations. We found that the

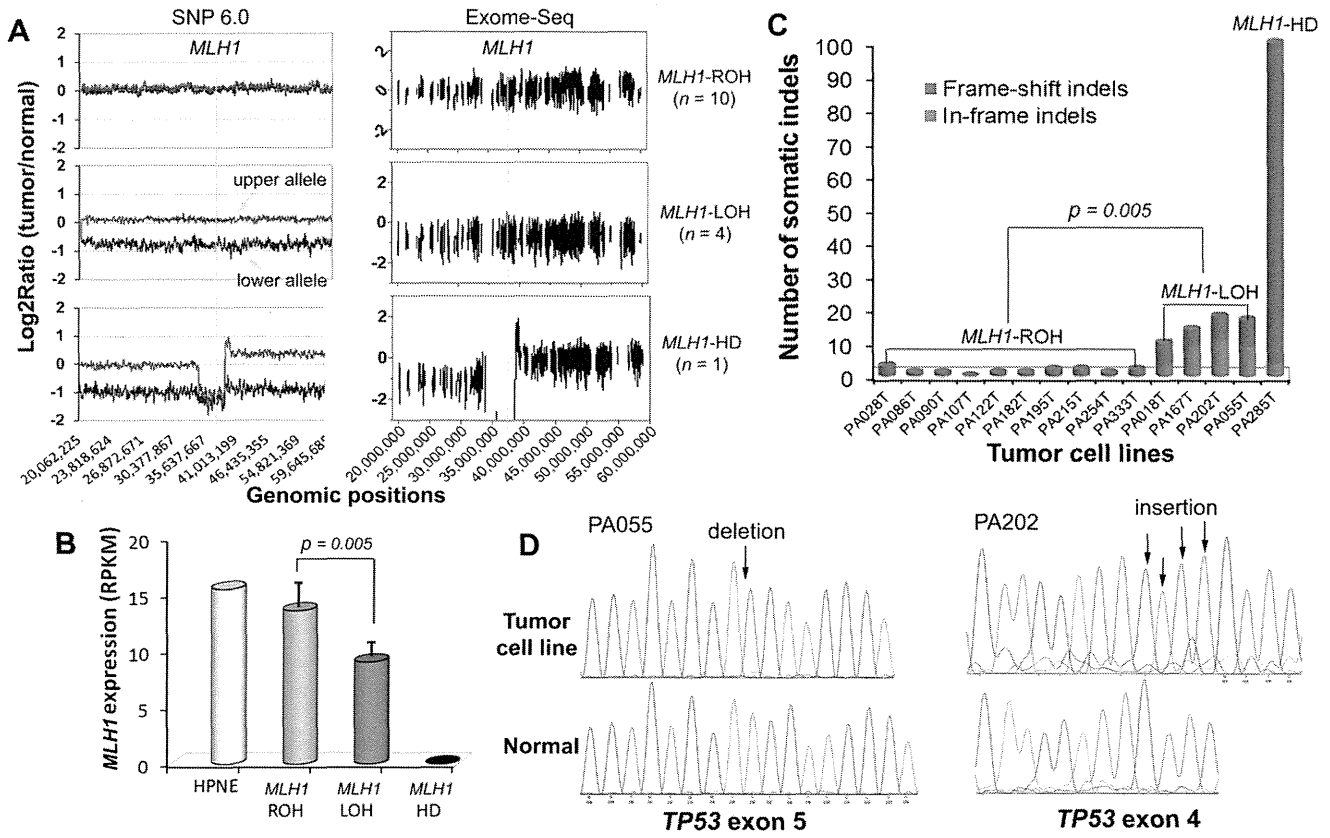

Figure 2. Allelic loss of *MLH1* and the increased rate of somatic indel mutations. (*A*) The distinct DNA copy-number status of *MLH1*. The *left* and *right* panels show the DNA copy-number status inferred from SNP array and Exome-seq data, respectively. The line in light blue indicates the approximate genomic location of *MLH1*. For graphs in the *left* panel, the *y*-axis indicates the adjusted $\log_2$ ratios of signal intensities between the tumor cell line and its matched normal sample for perfect match probes. The red line represents the allele with a higher copy number, and the blue line represents the allele with a lower copy number. The $\log_2$ ratio of −1 and 0 theoretically corresponds to 0 and 1 copy, respectively. For graphs in the *right* panel, the *y*-axis indicates the $\log_2$ ratios of the sequence coverage between the tumor cell line and its matched normal sample for targeted exonic regions. (*B*) The differential expression of *MLH1*. The gene expression level was examined by mRNA-seq. (*RPKM*) Reads per kilobase per million mapped reads. (Bars) Mean ± SD. (*C*) The somatic indels. The number of somatic small indels identified in the targeted exonic regions is shown for each tumor cell line. (*D*) Validation of the truncating indels identified in *TP53* in two *MLH1*-LOH cell lines. (*Left*) 1-bp deletion; (*right*) 4-bp insertion. The positions of indels are indicated by arrows in the sequence electropherograms.

gene *MLH1* was differentially expressed among the subgroups, and the expression levels appeared to be reversely correlated with the mutation rates. As shown in Figure 2B, the expression of *MLH1* decreased by nearly half in group-2 cell lines ($P = 0.005$) and was almost lost in the group-3 cell line. We did not observe any significant differences in the expression of other DNA MMR genes among the subgroups (Supplemental Fig. S9), nor did we detect somatic point mutations of other MMR genes in any of the cell lines. We then quantitatively measured the methylation status of the *MLH1* promoter using MassARRAY, but none of the cell lines showed promoter hypermethylation of this gene (Supplemental Fig. S10). We further examined DNA copy-number changes of *MLH1* and found a clue to its differential expression. As shown in the left panel of Figure 2A, cell lines in group 1 retained both alleles of *MLH1* (*MLH1*-ROH [retention of heterozygosity]), while cell lines in group 2 lost one of the two alleles of this gene (*MLH1*-LOH [loss of heterozygosity]); the cell line in group 3 lost both alleles (*MLH1*-HD [homozygous deletion]). The distinct DNA copy-number status of *MLH1* was also well demonstrated by the read-depth–based Exome-seq data (Fig. 2A, right panel).

Characterization of somatic indels in the *MLH1*-LOH and *MLH1*-HD cell lines

We identified an average of 1.4 ± 0.8 indels per *MLH1*-ROH cell line, 14.8 ± 3.5 indels per *MLH1*-LOH cell line, and 100 indels in the *MLH1*-HD cell line. The mutation rate of the somatic indels was 10.5- and 72.1-fold higher in *MLH1*-LOH and *MLH1*-HD cell lines, respectively, compared with that of the *MLH1*-ROH cell lines ($P = 0.005$) (Fig. 2C). Among the total of 173 somatic indels, 94 were detected in the coding microsatellites (Supplemental Table S1). Prevalence of the indels in the microsatellites was increased sixfold and 154-fold, respectively, in the *MLH1*-LOH and *MLH1*-HD cell lines. Nearly half of the indels that were detected in *MLH1*-LOH cell lines and the majority of indels that were detected in the *MLH1*-HD cell line were frame-shift mutations. Some of the frame-shift indels were present in cancer-related genes such as *TP53*, *BRCA2*, *TGFBR2*, and *MLL3* and were predicted to be protein truncating. We identified a 1-bp insertion in the poly(A)10 tract of *TGFBR2* in one of the *MLH1*-LOH cell lines and validated it by mRNA-seq. We detected two truncating indels in *TP53* in two other *MLH1*-LOH cell lines and validated them by both Sanger sequencing

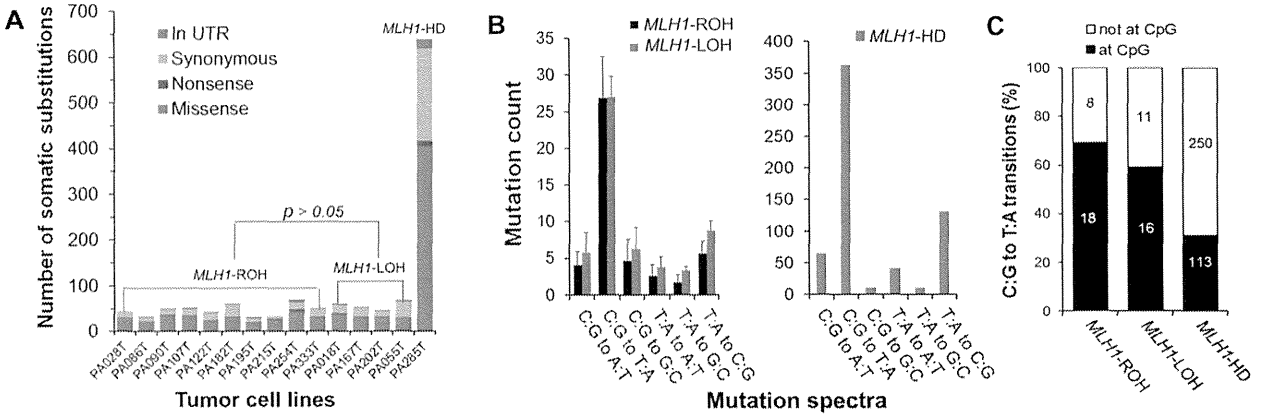

Figure 3. Characterization of the somatic base substitutions. (*A*) The number of somatic base substitutions. The *MLH1*-HD cell line showed a dramatically elevated mutation rate of somatic substitutions. (*B*) The pattern of mutation spectra. (*C*) The distribution of the C:G to T:A transitions at and not at the CpG dinucleotides. For *B*, the data are shown as mean ± SD. As for *C*, the mean values are marked on corresponding columns.

and mRNA-seq (Fig. 2D; Supplemental Table S1). Both indels were accompanied by LOH and introduced premature termination codons (PTCs), resulting in a dramatic reduction of *TP53* expression (Supplemental Fig. S11).

The mutation spectra

The pattern of mutation spectra was quite similar among the subgroups. As shown in Figure 3B, the predominant type of base substitution was the C:G to T:A transition, followed by the T:A to C:G transition. Many cancer genes such as *KRAS*, *TP53*, *SMAD4*, and *APC* were mutated by a C:G to T:A transition. In the *MLH1*-HD cell line, the mutation rate of the C:G to T:A transitions was markedly increased, especially at non-CpG sites (Fig. 3C). The frequency of other classes of base substitution was also dramatically higher except for the C:G to G:C and T:A to G:C transversions.

Evaluation of genomic instability using Exome-seq

Based on the Exome-seq data, we determined the microsatellite instability (MSI) status of *MLH1*-ROH, *MLH1*-LOH, and *MLH1*-HD cell lines as "stable," "intermediately unstable," and "highly unstable," respectively (Supplemental Table S1). We then performed the conventional MSI assay for the same sample set (Supplemental Fig. S12). The assay revealed that all seven markers were stable in the *MLH1*-ROH cell lines, and two of the markers, D17S250 and D2S123, were unstable in the *MLH1*-HD cell line. However, none of the markers showed instability in any of the *MLH1*-LOH cell lines. Using the conventional MSI assay, *MLH1*-LOH cell lines were indistinguishable from *MLH1*-ROH cell lines. To further evaluate the performance of Exome-seq, we selected three representative coding microsatellites, within which somatic indels have been identified by Exome-seq and validated by mRNA-seq. We designed fluorescence-labeled primers and performed the MSI assay. The conventional assay confirmed instability for all three microsatellites (Fig. 4).

Discussion

In this study, we analyzed 15 PDAC-derived cell lines and their matching normal tissues using Exome-seq. We detected more than 1500 point mutations and showed that 1359 genes were somatically altered in at least one of the cell lines. *KRAS*, *TP53*, *CDKN2A*, and *SMAD4*, known as the "master" genes for PDAC, were the top four most frequently mutated genes identified in this study. These results are consistent with an early study performed by Jones and colleagues (2008) using the Sanger sequencing method, indicating a good performance of Exome-seq, as well as our mutation detection pipeline.

Mutation of the four key players, although being of paramount importance, may not be sufficient to drive the development and progression of PDAC, since variability can occur among tumors arising in the same organ and among cell populations within the same tumor. Recent studies have reported the intertumoral heterogeneity among PDACs and the intratumoral heterogeneity in a hepatocellular carcinoma (Kim et al. 2011; Totoki et al. 2011). The number of mutated genes that drive development of cancer was found to be far greater than previously thought (Greenman et al. 2007). By using Exome-seq, we identified additional 52 genes that recurrently mutated in PDAC. Among them, the mutation of 41 genes has not been described in this cancer type. More than half of these genes have been suggested to play a role in carcinogenesis. For example, a recent study showed *NFE2L2* is frequently mutated in lung cancers (Shibata et al. 2010). The overexpression of *SOX5* is associated with prostate tumor progression and early development of distant metastasis (Ma et al. 2009). *EXOC8* has been shown to foster oncogenic Ras-mediated tumorigenesis (Issaq et al. 2010). Mutation screening of these genes in a large sample size would help us gain a further understanding of their biological contribution to PDAC.

The application of NGS technologies to cancer genomics has dramatically increased the efficiency of mutation discovery. Since a variety of factors, such as sequencing platforms, data mapping, and variant calling algorithms can affect the final output of identified mutation candidates, validation of the numerous proposed mutations has consequently become a common issue to be considered. We here evaluated the performance of mRNA-seq in verification of mutations identified in coding regions. If we simply consider all somatic mutations identified by Exome-seq, 61.6% of them were validated by mRNA-seq. If we focus, however, on those mutations in expressed genes, 94.3% of them can be successfully confirmed by mRNA-seq. For truncating mutations, despite a lower abundance of the mutant allele in cDNA, mRNA-seq was still able to confirm 86.2% of the mutations. This suggests that although it may miss mutations in poorly expressed regions, mRNA-seq may

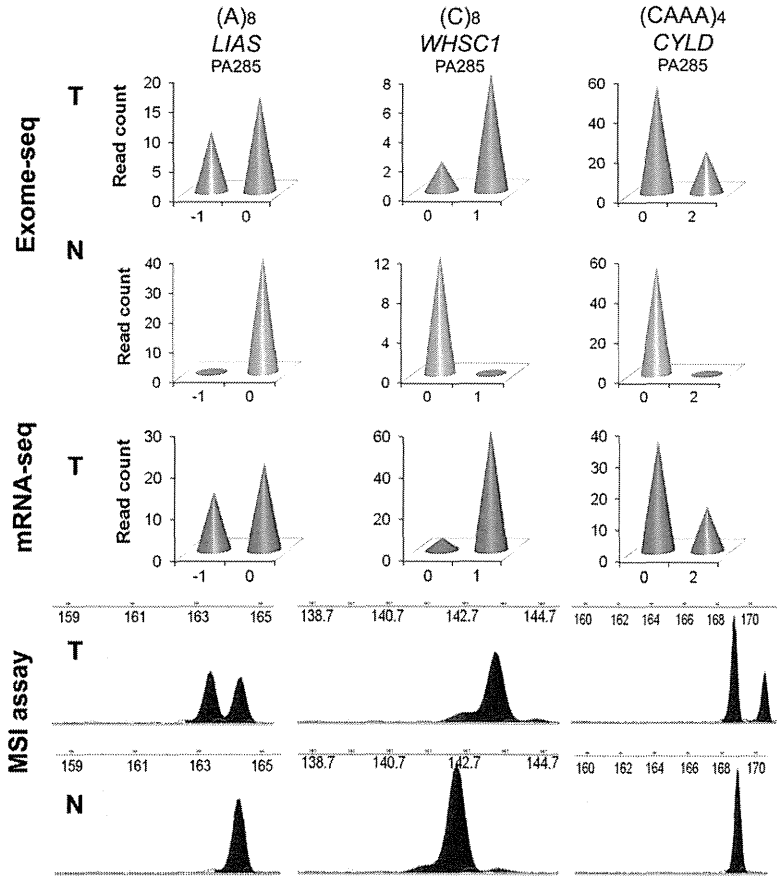

Figure 4. MSI analysis using Exome-seq. The data for three representative microsatellites are shown. (*Top*) Read-depth based Exome-seq data; (*middle*) mRNA-seq data; (*bottom*) electropherograms of the conventional MSI assay. For the *top* and *middle* panels, the *x*-axis indicates the lengths of indels. The negative value indicates base deletion, and the positive value indicates base insertion, while 0 indicates no indel. The numbers marked at the *y*-axis indicate the number of sequence reads that carry the mutant allele or the wild-type allele. (*Bottom*) *x*-axis is the size in bases; *y*-axis is the fluorescence intensity. The red peaks are internal size standards.

be a workable alternative to Sanger sequencing for the validation of mutations identified in expressed genes. In addition to learn about gene expression and splicing variants, groups who run NGS on both gDNA and cDNA for the same sample set may get an extra benefit from such an application.

Allelic loss at the short arm of chromosome 3 is one of the most common genetic alterations observed in human cancers. It has been reported in over 30% of PDAC and nearly 90% of RCC cases (Yamano et al. 2000; Harada et al. 2008; Toma et al. 2008). Many potential cancer genes have been identified on chromosome 3p. The DNA MMR gene *MLH1* is located at chromosome 3p22.2. In mammals, the MLH1 protein is an essential component of the MMR complex. MLH1 protein binds to either PMS1 or PMS2, and both heterodimers bind either to the MSH2/MSH6 heterodimers to correct mismatches or to the MSH2/MSH3 heterodimers to correct indel errors (Jiricny 1998; Kolodner and Marsischky 1999; Raschle et al. 1999). Among the MMR proteins, the loss of MLH1 is by far the most common cause of MSI. To date, a variety of genetic and epigenetic alterations in *MLH1* has been discovered in many different types of cancers (Bronner et al. 1994; Cunningham et al. 1998; Kuismanen et al. 2000; Suter et al. 2004; Arnold et al. 2009). In pancreatic cancers, the mutation of *MLH1* and MSI has been reported in a histologically distinct subset of poorly differentiated adenocarcinomas, called medullary carcinomas, which usually have a wild-type *KRAS*. The sporadic PDAC, however, seldom, if ever, has MSI (Wilentz et al. 2000). To our knowledge, the profile of MSI has yet to be fully demonstrated in a genome-wide manner in pancreatic cancers.

Homozygous deletion of *MLH1* is a rare case and has not been documented previously. In one of the cell lines analyzed in this study, we incidentally detected a focal homozygous deletion spanning the entire *MLH1* locus. Exome-seq revealed intensive genomic instability in this cell line, indicated by a dramatically elevated mutation rate of somatic substitutions, small indels, as well as the indels presented in coding microsatellites. The number of C:G to T:A transitions was markedly increased, especially at non-CpG sites, suggesting an impaired recognition/repair of G:T mismatches (Marra and Schar 1999; Kumar et al. 2009). The mutation spectrum of the cell line was quite similar to that of other types of MMR-deficient tumors previously reported (Greenman et al. 2007).

Although allelic loss of *MLH1* has been reported in over 30% of PDACs (Yamano et al. 2000; Harada et al. 2008), no statistical correlation has been described between *MLH1* allelic loss and an increased mutation rate. It was previously thought that mutations in *MLH1* and other DNA MMR genes are recessive; i.e., a single copy of the wild-type *MLH1* allele is sufficient to perform its normal function (Bodmer et al. 2008; Negrini et al. 2010). In this study, we notably found that *MLH1* expression was decreased by nearly half in cell lines with an allelic loss of *MLH1*. While these cell lines were negative in a conventional MSI assay, they showed a 10.5-fold increase in the rate of somatic indels. We also observed a higher prevalence of indels in the coding microsatellites. Moreover, we identified truncating indels that inactivate tumor suppressor genes, such as *TP53* and *TGFBR2*. These results indicate that deletion of one copy of *MLH1* gene results in haploinsufficiency in the correction of DNA indel errors.

An earlier study performed in vitro could support our argument that hemizygous deletion of *MLH1* may lead to an impaired DNA repair and genomic instability. Edelmann and colleagues (1996) generated mice with a null mutation of the *MLH1* gene and measured the MMR activity in vitro using the cell-free extracts from the mouse embryo-derived fibroblast (MEF). They found that the embedded errors in the reporter gene were repaired 2.3-fold less efficiently in MEF extracts of $mlh1^{+/-}$ mice compared with that of $mlh1^{+/+}$ mice.

To further address the significance of *MLH1* hemizygous deletion in in vivo tumors, we examined the primary RCC samples, which usually exhibit LOH on chromosome 3p. All patients provided informed consent for the research use of their samples, and

the study was approved by the institutional review board of the National Cancer Center Research Institute. We enriched the exonic sequences of 15 primary RCCs and their matched normal samples using the Agilent Human All Exon 50 Mb Kit and sequenced the exomes using the HiSeq 2000 sequencing system. Among the 15 RCCs analyzed, 13 cases showed LOH at the *MLH1* locus on chromosome 3p, and two cases showed ROH. The data are shown in Supplemental Figure S13 and Supplemental Table S3. On average, we identified 1.5 somatic indels in the *MLH1*-ROH cases, which is consistent with a previous report (Varela et al. 2011). However, in the *MLH1*-LOH tumors, we observed a 4.6-fold increased rate of somatic indel mutations ($P = 0.0008$). A total of 90 somatic indels were identified in 13 *MLH1*-LOH cases. Among them, 85 were frame-shift indels and 68 were truncating indels. Moreover, we detected recurrent truncating indels in several well-characterized cancer genes, such as *VHL* (four cases), *PBRM1* (four cases), and *JARID1C* (four cases). These data suggest that the correlation we observed between *MLH1* allelic loss and the increased mutation rate of somatic indels is more likely to be the true rather than a simple coincidence. Our data also indicate that *MLH1* allelic deletion, through increasing the frequency of somatic indel mutations in cancer genes, could drive the development and progression of cancer. It is potentially significant that the correlation we observed was only with somatic indels, and not base substitutions. Presumably, MLH1 protein may play a pivotal role in correction of DNA indel errors, while its function for MMR can be partially compensated by other MMR proteins or mechanisms. Nevertheless, we could not exclude the possibility that factors that predispose to DNA copy-number losses might also associate with indel frequency.

In human cancers, LOH at chromosome 3p is frequently observed (Yamano et al. 2000; Harada et al. 2008; Toma et al. 2008). However, the association between *MLH1* allelic loss and the increased rate of somatic indel mutations has not been notified. There are several possible reasons. First, depending on the platform, sequencing indels can be difficult. Second, reads arising from indel sequence are generally more difficult to be aligned to the reference genome. Without a good coverage, indels are more difficult to be detected. Third, the MSI assay is conventionally used to evaluate the occurrence of indels at microsatellites as genome-wide mutation analysis was not available until recently (Boland et al. 1998). The MSI assay is insufficient since only several microsatellites are selected. In addition, technical limits exist in the conventional assay (Hatch et al. 2005; Fujii et al. 2009). For example, the assay system employs capillary electrophoresis and autoradiography, making it sometimes difficult to recognize small changes in the microsatellite sequences. Some artificial fragment peaks were usually introduced after 32 cycles of PCR amplification. The choice of markers may also affect the sensitivity of the assay (Hatch et al. 2005; Fujii et al. 2009). In contrast, our data suggest that Exome-seq may be an acceptable alternative for microsatellite analysis.

Methods

The samples

PDAC-derived cell lines

We analyzed a total of 15 PDAC-derived cell lines and their matched normal samples. Primary pancreatic tumor tissue contains a high admixture of contaminating non-neoplastic inflammatory and stromal cells. To remove the non-neoplastic cells and facilitate the detection of somatic mutations, microdissected primary tumors were passaged in vitro as cell lines prior to extracting DNA and RNA for sequence analysis. The characteristics of the PDAC-derived cell lines are listed in Table 1. All cell lines were established by researchers at the Cancer Institutes, Japanese Foundation of Cancer Research (JFCR). The matching normal tissues were surgically resected from tumor-negative pancreas. All normal samples were histologically reviewed by two pathologists and were confirmed to be free of tumor tissues. All patients provided informed consent for the research use of their samples, and the study was approved by the institutional review board of the JFCR and the University of Tokyo. The DNA and RNA were extracted by standard protocols. The pair matching of each tumor cell line and the normal sample was confirmed by genome-wide SNP array (Affymetrix).

HPNE cell line

The human telomerase reverse transcriptase (hTERT)-immortalized pancreas duct epithelial cell line (hTERT-HPNE, CRL-4023) was purchased from The American Type Culture Collection (ATCC). The cells were cultured in low-glucose DMEM media (Invitrogen) supplemented with 25% Medium M3 Base (Incell), 5% fetal bovine serum, and 10 ng/mL human recombinant epithelial growth factor (Sigma Aldrich) at 37°C and with 5% carbon dioxide. HPNE serves as the normal control for gene expression analysis.

Exome-seq and data analysis

Exome-seq

Targeted enrichment was performed with Agilent SureSelect Human All Exon Kit V1.0 (Agilent Technologies). This kit is designed to enrich 162,073 exons of 16,954 protein-coding genes, more than 700 microRNAs and 300 noncoding RNAs, covering ~37.6 Mb of the human genome (Supplemental Fig. S14). SureSelect Biotinlyated RNA baits were designed to be 120-mer long and end-to-end tiled (1× tilling). The gDNA libraries were prepared using an Illumina paired-end DNA sample prep kit (Illumina) following the manufacturer's protocols with slight modifications. In brief, 3 μg gDNA was fragmented using Covaris Acoustic Solubilizer (Covaris) with 20% duty cycle, 4 intensity, and 200 cycles per burst for 160 sec, at 16°C to get DNA fragments with a mean size of 200 bp. Fragmented DNA was then purified using Agencourt AMPure XP magnetic beads (Beckman Coulter). The concentration of the library was measured using a Bioanalyzer (Agilent Technologies). The adapter-ligated libraries were amplified with six PCR cycles, and 500 ng of each amplified library was hybridized with Biotinlyated RNA baits in solution for 24 h for target enrichment. Subsequently, hybridized libraries were cleaned up and further amplified with 12 cycles of PCR; 5–6 pM/lane DNA was applied to the flow cell, and paired-end 76-nucleotide (nt)-long reads were generated using the Illumina Genome Analyzer IIx Platform (GAIIx). Each sample was run on a single lane of Illumina flow cell except for samples PA028N and PA167T, which were each run on two lanes.

Data alignment and variant calling

The detail workflow for data alignment and mutation detection was described in Supplemental Figure S15. For each cell line and matched normal sample, the sequence reads were mapped to the human NCBI Build 36 reference sequence (hg18, downloaded from http://genome.ucsc.edu) initially with the Illumina sequencing pipeline (version 1.6) for quality recalibration. The passing filter (PF) reads were then mapped again using BWA (version 0.5.8) (Li and Durbin 2009). Any potential PCR duplicates, ambiguous reads, inconsistent read pairs, and singletons were excluded. Only the unique reads that mapped in consistent read pairs (with proper insert size and orientations) were selected for further

analysis. The bases substitutions were called using SAMtools (version 0.1.7) (Li et al. 2009), and the indels were called using both SAMtools and Pindel algorithms (Ye et al. 2009).

Variant filtering and somatic variant identification

To pick out the high-confident somatic variants, we applied the following rigorous filters and rules to the data set (Supplemental Fig. S15). The first filter applied is the "quality filter." Variants with a mapping quality of 20 or more, a *phred*-like consensus quality of 20 or more, a base call quality of more than 10, and a sequence coverage of 10× or more for both the cell line and matched normal sample were considered as high-quality variants. The setting for the filter conditions were optimized by comparing common SNPs detected by BWA (Li and Durbin. 2009) with those genotyped using Affymetrix Human SNP Array 6.0 (Affymetrix), ensuring a high concordance (99.84%) across two analyses (Supplemental Fig. S16).

The second filter applied, referred to as the "somatic filter," seeks to pick out the somatically acquired variants. All the high-quality variants produced from the above steps were passed through the "somatic filter," and only those meeting the threshold were considered as the somatic variants. The mutant allele (nonreference allele) ratio was calculated as follows:

$$\textit{Mutant allele ratio} = \frac{\text{Count of non-reference bases}}{\text{Count of total bases}} \times 100\%$$

The setting for the "somatic filter" is as described in Supplemental Figure S15; for the cell line sample, it is required that four or more reads supporting the mutant allele and the mutant allele ratio should be 15% or more. Moreover, the mutant allele should be supported by reads that aligned in both the forward and reverse directions. For the matched normal sample, given the potential sequencing errors and mapping errors, the mismatch should not be detected in more than 3% of the aligned reads and should not be detected in more than two reads. The indel, however, should not be detected in any of the aligned reads.

The third filter, referred to as the "false-positive filter," was then applied. This filter is used to remove the potential false-positive events that result from the homologous sequences within the human genome, mapping errors, and so on. For each of the somatic mutations produced in the above steps, we extracted 200–300 bases of DNA sequences flanking its mutation locus and mapped the sequences to hg18 using the BLAT algorithm. Subsequently, the mutations identified within the regions rich for homologous sequences were removed from the list. The somatic mutations were further examined using the integrated genome viewer (IGV), and any mutations found in a "noisy" background (multiple mismatches or indels in flanking sequences) were removed from the list.

As for detection of indels, one more step, called "rescue," was applied since the sequence read carrying a long indel toward its end is usually difficult to be aligned properly. We use the Pindel algorithm to rescue those possibly missed indels.

Variant annotation

Functional effects of filtered somatic variants were predicted using the SIFT algorithm (Kumar et al. 2009; http://sift.jcvi.org). The SIFT algorithm predicts whether an amino acid substitution affects protein function based on sequence homology and the physical properties of amino acids.

Mutation rate calculation and normalization

The background mutation rate (mutations/per Mb coding sequences) was calculated as follows:

$$\frac{\text{Sum of somatic mutations}}{\text{Sum length of exome targets} \times \text{number of tumor cell lines}}$$

The mutation rate of each gene was normalized by the frequency of mutations and the length of its coding sequences. Only somatic deleterious mutations, including missense substitutions, nonsense substitutions, frame-shift indels, and focal homozygous deletions were counted. The normalized mutation rate for each gene was calculated as follows, and a priority list was made accordingly:

$$\frac{\text{Sum of somatic mutations identified in the gene}}{\text{Sum length of coding regions of the gene} \times \text{number of tumor cell lines}}$$

Pathway analysis

The genes with somatic mutations were classified into different functional pathways using the Gene Ontology (GO) database (http://www.geneontology.org/). Only somatic deleterious mutations were counted. The normalized mutation rate for each pathway was calculated as below:

$$\frac{\text{Sum of somatic mutations identified in genes included}}{\text{Sum length of coding regions of genes included} \times \text{number of tumor cell lines}}$$

mRNA-seq and data analysis

Library preparation and mRNA-seq

Total RNA was extracted from PDAC-derived cell lines and the HPNE cells using the protocol outlined in the RNeasy Kit (Qiagen). Total RNA integrity was measured using a 2100 Bioanalyzer (Agilent Technologies), and all samples were confirmed to have an RNA Integrity Number (RIN) greater than 8.0 prior to further analysis. The mRNA-seq libraries were prepared using a paired-end mRNA Sequencing Sample Prep Kit (Illumina) following the manufacturer's protocols with slight modifications. Briefly, 2 μg of total RNA was used as the starting material, and the polyadenylated RNAs were selected using Sera-Mag Magnetic Oligo(dT) Beads (Illumina). The Poly(A)$^+$ RNA was then fragmented by heating for 90 sec at 94°C in the supplied fragmentation buffer. Fragmented RNA was mixed with random primers, incubated for 5 min at 65°C, and placed on ice briefly before starting cDNA synthesis. First-strand cDNA synthesis was performed using SuperScript II, and second-strand cDNA synthesis was performed using DNA Pol I in the supplied GEX second-strand reaction buffer. Subsequently, cDNA ends were repaired, and adenine was added to the 3′ end of the cDNA fragments to allow adaptor ligation. Paired-end adaptors were ligated to the cDNA fragments. The ligated product was run on a 2% agarose gel, and a 300 ± 20 bp fragment was cut out and extracted. PCR (eight cycles) was performed with Phusion High-Fidelity DNA Polymerase (Finnzymes Oy) following the manufacturer's protocols. The PCR products were cleaned up with Agencourt AMPure XP magnetic beads (Beckman Coulter); 6.0–6.7 pM/lane cDNA was applied to the flow cell and paired-end 76-nt-long reads were generated using Illumina GAIIx. Each sample was run on two lanes of Illumina flow cell.

Data alignment

All PF reads were aligned to hg18 using TopHat spliced aligner (Trapnell et al. 2009). Meanwhile, all PF reads were aligned to NCBI Reference Sequence (RefSeq) mRNA sequences using BWA. A merged file was generated for each sample by integrating the output of